

Ferroelectric soft mode and microwave dielectric relaxation in $\text{BaTiO}_3\text{-PbMg}_{1/3}\text{Nb}_{2/3}\text{O}_3$ ceramicsV. Bovtun¹, D. Nuzhnyy¹, M. Kempa¹, T. Ostapchuk¹, V. Skoromets¹, J. Suchanicz²,
P. Czaja², J. Petzelt¹ and S. Kamba¹¹Institute of Physics of the Czech Academy of Sciences, Prague 182 21, Czech Republic²Institute of Technology, Pedagogical University, Cracow 30-084, Poland

(Received 2 September 2020; revised 10 November 2020; accepted 22 December 2020; published 12 January 2021)

BaTiO_3 (BT) is the best-known ferroelectric and $\text{PbMg}_{1/3}\text{Nb}_{2/3}\text{O}_3$ (PMN) is the best-known relaxor ferroelectric, but their solid solutions were so far studied only very scarcely. Here the high-density perovskite ceramic solid solutions of $(1-x)\text{BaTiO}_3\text{-}x\text{PbMg}_{1/3}\text{Nb}_{2/3}\text{O}_3$ (BT-100x%PMN, $x = 0.075, 0.10, 0.15$) were studied by the infrared reflectivity, time-domain terahertz transmission and microwave spectroscopies (1 MHz–20 THz) and compared with the undoped BT and PMN ceramics. The spectra show presence of a split soft phonon at all temperatures, similar to that observed in BT and PMN. Microwave dielectric dispersion was observed both below and above temperature of the diffuse permittivity maximum. In the case of BT-7.5%PMN and BT-10%PMN, the main dispersion takes place above 1 GHz, in case of the BT-15%PMN, the dispersion covers more homogeneously the 1 MHz–1 THz range. The dielectric response up to the THz range of the BT-10%PMN and BT-15%PMN was fitted with three excitations: soft mode, central mode (lower-frequency component of the split soft phonon), and microwave relaxation, but the soft mode does not soften appreciably and only the latter two excitations contribute substantially to the dielectric permittivity maximum. Dielectric response of the BT-7.5%PMN is similar except for the presence of a second dielectric relaxation in the MHz range, also observed in BT. The relaxations show no PMN-like freezing and can be tentatively attributed to the dynamics of polar nanoregions in the paraelectric phase and to the domain/nanodomain wall dynamics and/or acoustic wave emission and piezoelectric resonances within the grains in the ferroelectric phase. In this way, the BT-100x%PMN ceramics cannot be considered as relaxor ferroelectrics, but rather as ferroelectrics with the diffuse phase transition. The broadband dielectric spectra of undoped BT ceramics revealed a split optical soft mode and two additional dielectric relaxations which are mainly responsible for the dielectric anomaly at the ferroelectric phase transition. It supports the phase transition in BT to be at the crossover from a displacive to an order-disorder type.

DOI: [10.1103/PhysRevMaterials.5.014404](https://doi.org/10.1103/PhysRevMaterials.5.014404)

I. INTRODUCTION

Lead-based perovskite (ABO_3) ferroelectrics form a large class of technologically important materials. Much of them are $\text{PbMg}_{1/3}\text{Nb}_{2/3}\text{O}_3$ (PMN)-based compounds. Despite their outstanding piezoelectric properties, these materials are currently facing global restrictions due to the Pb toxicity. Therefore, development of the lead-free or low-lead substitutes that can compete with the PMN-based materials is an actual problem [1,2]. BaTiO_3 -PMN (BT-PMN) system with low PMN content could be considered as a possible alternative to the lead-based compounds which are known as excellent piezoelectrics, capacitors, and nonlinear dielectric materials and therefore are widely used in electronics. Our preliminary piezoelectric measurements of BT-PMN found relatively high piezoelectric parameters: $d_{33} = 150\text{--}210$ pC/N and $k_{33} = 60\text{--}70\%$, which makes this material perspective for the high-frequency applications in piezoelectric transducers and actuators. There are, however, very few reports in the literature on the effect of PMN adding to the properties of BT [3–5]. Above all, it was shown that addition of BT to PMN favors formation of the perovskite phase over the unwanted pyrochlore phase in the sintered material [3,5].

The BT-PMN system combining ferroelectric and relaxor components looks interesting also from the physics point of

view. BT is the most extensively studied ferroelectric material with many actual and potential applications. It has a cubic structure ($Pm\bar{3}m$) at high temperatures. On decreasing temperature, the phase transition to ferroelectric tetragonal phase ($P4mm$) occurs at ~ 400 K. The transition is of the first-order predominantly displacive with many features involving also an order-disorder mechanism [6–9]. On further decreasing temperature, another first-order ferroelectric phase transition to orthorhombic phase ($Amm2$) takes place at ~ 280 K and finally the rhombohedral structure ($R3m$) appears below ~ 180 K [10]. The corresponding spontaneous polarization P_s changes stepwise from (001) to (110) and (111) directions, respectively.

PMN is a model relaxor ferroelectric with cubic symmetry ($Pm\bar{3}m$) in the entire temperature range [11] which exhibits a pronounced diffuse and frequency-dependent maximum of the dielectric permittivity near ~ 270 K and Vogel-Fulcher-type freezing temperature $T_f \approx 210$ K [12]. More recently, an intermediate temperature $T^* \approx 400$ K was introduced, which corresponds to temperature where the split soft phonon mode achieves its minimum frequency [13,14]. Below the T_f , external electric field can induce a quasistable ferroelectric phase [15]. The relaxor-type dielectric dispersion is due to dynamic polar nanoregions which appear below the Burns temperature

$T_d \approx 650$ K as the consequence of the correlated ion off-center displacements: B-site ions are shifted along the (111) direction by about 0.18 Å, while the Pb off-center displacements show a larger spherically symmetric distribution with a mean diameter of 0.33–0.4 Å [16–20].

Unlike PMN, where the relaxor behavior originates mainly from the more off-centered Pb ions at the A sites, in the classical ferroelectric BT, the ferroelectricity originates in gradual displacement or ordering of the off-centered Ti ions at the B sites [6]. In PMN, the B-site order is also disturbed due to the different valences and ionic radii of the B-site ions, resulting in formation of so-called chemical clusters and random electric fields. However, it also induces the polar clusters due to locally ordered Pb clusters at the A sites. Both types of clusters develop rather independently of each other [21]. Therefore, also in the BT-PMN system it can be expected that the competition between the A- and B-site disorder and off-centering should play an important role.

Structural, low-frequency dielectric, ferroelectric, thermoelectric, and Raman properties of the ceramic solid solutions of $(1-x)\text{BaTiO}_3-x\text{PbMg}_{1/3}\text{Nb}_{2/3}\text{O}_3$ (BT-PMN or BT-100x%PMN) with $x \leq 0.15$ were studied by Suchanicz *et al.* [22,23]. Evolution of the low-frequency dielectric behavior from the ferroelectric BT-like towards the relaxorlike one on increasing the PMN content was revealed. According to the phase diagram, all three phase transitions typical for BT were present in ceramics with $x \leq 0.05$, while only two transitions (from cubic to tetragonal and to rhombohedral phase on cooling) were observed in compositions with $x = 0.075, 0.10$, and only one from the cubic to rhombohedral phase in the composition with $x = 0.15$. No high-frequency dielectric nor terahertz (THz) and infrared (IR) spectroscopy studies have been reported so far.

For studying the crystal lattice dynamics of BT-100x%PMN we have chosen three ceramic compositions with $x = 0.075, 0.10$, and 0.15 for our dielectric experiments in the microwave (MW), THz, and IR ranges, and present here their broadband high-frequency dielectric response (1 MHz–20 THz) in comparison with a similar response of the pure BT coarse-grain (grain size ~ 10 μm) ceramics [24–27] and PMN ceramics and crystals [13,14,28].

II. EXPERIMENTAL DETAILS

Depending on the processing conditions, the unwanted pyrochlore structure in addition to the perovskite one may be present in lead-based ceramics (particularly in PMN and PMN-based materials), which deteriorates their dielectric and ferroelectric properties [29]. It is rather difficult to prepare pure PMN and PMN-based ceramics with a high content of PMN pyrochlore-free phase via the conventional solid-state route. Pyrochlore-free high-density (>95%) BT-7.5%PMN, BT-10%PMN, and BT-15%PMN ceramics were prepared by a two-step conventional solid-phase sintering [22,23]. Structural (x-ray diffraction) and microstructural (scanning electron microscopy) characterization [22,23] proved the perovskite structure with absence of secondary phases, showed the average grain size of 2.5–4.5 μm, and allowed construction of the phase diagram [22].

IR reflectivity spectra were measured at near-normal incidence using Fourier transform IR spectrometer Bruker IFS 113v equipped with pyroelectric deuterated triglycine sulfate detector and Si bolometer (operating at 1.6 K) for high- and low-temperature measurements, respectively. In the THz range, the complex dielectric spectra were obtained using the time-domain THz transmission spectrometer based on a Ti:sapphire femtosecond laser [30]. An interdigitated photoconducting GaAs switch was used for generating the THz pulses. The transmitted THz pulses were detected using a plate of the [110]-oriented ZnTe crystal for the electro-optic sampling. In both experiments the Optistat continuous-flow cryostat with Mylar (for THz) and polyethylene (for IR) windows for low-temperature measurements and the high-temperature cell SPECAC P/N 5850 were used.

Two techniques were applied for dielectric measurements in the MW range. Complex input impedance of the shorted coaxial line with the rod-shaped cylindrical sample (~ 6.5 mm long and ~ 1 mm in diameter), inserted in the gap between the inner conductor and short, were measured at 1 MHz–1 GHz frequencies and 100–450 K temperatures. Gold electrodes were evaporated on the flat sample surfaces. A computer-controlled dielectric spectrometer consisting of the Agilent 4291B RF impedance analyzer, Novocontrol BDS 2100 coaxial sample cell, and Sigma Systems M18 temperature chamber with liquid nitrogen cooling was used for recording of the impedance spectra on cooling with a temperature rate of 1 K/min. The complex dielectric permittivity was calculated accounting for the electromagnetic field distribution in the sample. The composite dielectric resonator method [31–33] was used for the dielectric measurements at ~ 5.8 GHz. $\text{TE}_{01\delta}$ resonance frequency, quality factor, and insertion loss of the base cylindrical dielectric resonator with and without the sample were recorded during heating from 10 to 400 K with a temperature rate of 0.5 K/min in a Janis closed-cycle He cryostat. Thin disk-shaped samples without electrodes (the same as for the THz experiment) were placed on top of the base resonator. The resonators were measured in the cylindrical shielding cavity using the transmission setup with a weak coupling by Agilent E8364B network analyzer. Dielectric parameters of the samples were calculated from the measured resonance frequencies and quality factors of the base and composite resonators.

III. MW AND THz DIELECTRIC PROPERTIES

Temperature dependences of the MW dielectric permittivity (ϵ') and loss (ϵ'') of the BT-PMN, PMN, and BT ceramics are presented in Fig. 1. In agreement with the phase diagram [22], BT-7.5%PMN and BT-10%PMN show two diffuse anomalies of the MW dielectric parameters corresponding to the cubic-tetragonal (at ~ 320 and ~ 300 K) and tetragonal-rhombohedral (at ~ 230 and ~ 200 K) phase transitions on cooling, respectively. BT-15%PMN ceramics shows only one anomaly corresponding to the cubic-rhombohedral phase transition at ~ 225 K. Sharp anomalies in the MW dielectric permittivity and loss of BT ceramics reflect its three first-order phase transitions.

In the case of BT ceramics, relevant MW dielectric dispersion is observed mainly in the ferroelectric phases below

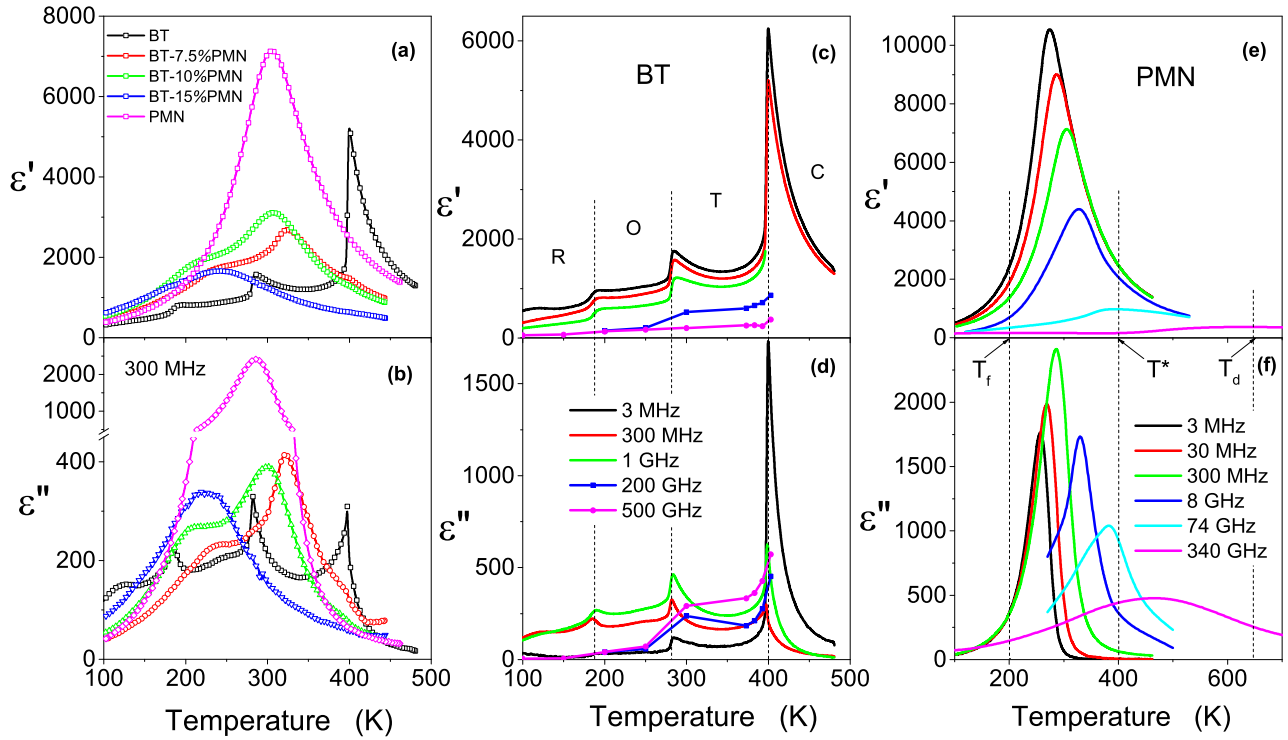


FIG. 1. Temperature dependences of the dielectric permittivity and loss at selected frequencies: (a), (b) BT (based on our data in Refs [24–27], BT-7.5%PMN, BT-10%PMN, BT-15%PMN ceramics and PMN crystals (based on our data in Refs. [13,14]) at 300 MHz; (c), (d) BT ceramics; (e), (f) PMN crystals. In (c), temperature regions of the ferroelectric rhombohedral (R), orthorhombic (O), and tetragonal (T) phases and cubic (C) paraelectric phase are denoted. In (e), characteristic temperatures (freezing T_f , T^* , and Burns T_d) are shown.

400 K [Figs. 1(c) and 1(d)]. The dispersion covers a broad frequency range between MHz and THz, and its substantial part takes place above 1 GHz. The $\epsilon'(T)$ and $\epsilon''(T)$ maxima do not shift on increasing frequency at least up to 1 GHz, and strictly correspond to the phase transition temperatures. Similar MW dielectric dispersion, substantial below 500 K, is also observed in all the BT-PMN samples (Fig. 2). Again, the main $\epsilon'(T)$ maximum does not shift remarkably on increasing frequency up to 1 GHz, unlike in the relaxor PMN [13]. For BT-7.5%PMN and BT-10%PMN, the main dispersion takes place above 1 GHz, similar to BT ceramics. In the case of BT-15%PMN, the dispersion covers the whole MW range, similar to PMN.

IV. ANALYSIS OF THE IR AND THz DIELECTRIC RESPONSE

IR reflectivity and THz complex dielectric spectra of the BT-PMN and BT ceramics were simultaneously fitted (using data on BT ceramics [24]) in a broad temperature range 10–900 K using the standard factorized formula of the generalized multioscillator dielectric function previously applied to BT and Ba(Zr, Ti)O₃ [24,26]:

$$\begin{aligned} \epsilon_{IR}^*(\omega) &= \epsilon'_{IR}(\omega) - i\epsilon''_{IR}(\omega) \\ &= \epsilon_\infty \prod_j \frac{\omega_{LOj}^2 - \omega^2 + i\omega\gamma_{LOj}}{\omega_{TOj}^2 - \omega^2 + i\omega\gamma_{TOj}}, \end{aligned} \quad (1)$$

related to the normal reflectivity spectrum by the Fresnel formula

$$R(\omega) = \left| \frac{\sqrt{\epsilon_{IR}^*(\omega)} - 1}{\sqrt{\epsilon_{IR}^*(\omega)} + 1} \right|^2, \quad (2)$$

where ϵ_∞ is the optical (electronic) contribution to the permittivity, ω is the linear frequency (wave number), ω_{TOj} and ω_{LOj} are the frequencies of the j th transverse (TO) and longitudinal (LO) optic phonon modes, and γ_{TOj} and γ_{LOj} are their damping parameters.

IR and THz reflectivity spectra of the BT-7.5%PMN, BT-10%PMN, and BT-15%PMN are similar and show presence of the split lowest-frequency soft phonon mode (SM), resembling that observed in BT [24,26] and PMN [13,14]. Figure 3 shows the reflectivity spectra for the BT-10%PMN and BT-15%PMN ceramics, while Fig. 4 for comparison presents the reflectivity spectra of BT and PMN ceramics and their fits using Eqs. (1) and (2). In Fig. 5 we plot the complex dielectric spectra of BT-10%PMN and BT-15%PMN in the range above 3 cm^{-1} (90 GHz) at selected temperatures as calculated from fit to reflectivity in Fig. 3 using Eqs. (1) and (2). Two components of the split overdamped SM above T_C are seen as broad overlapped loss maxima in the dielectric spectra below $\sim 50 \text{ cm}^{-1}$. The higher-frequency component is marked as SM, the lower-frequency one as central mode (CM). For comparison with BT and PMN, in Fig. 6 we plot similar spectra of BT and PMN ceramics, as calculated from our published IR-THz data [13,14,24,26].

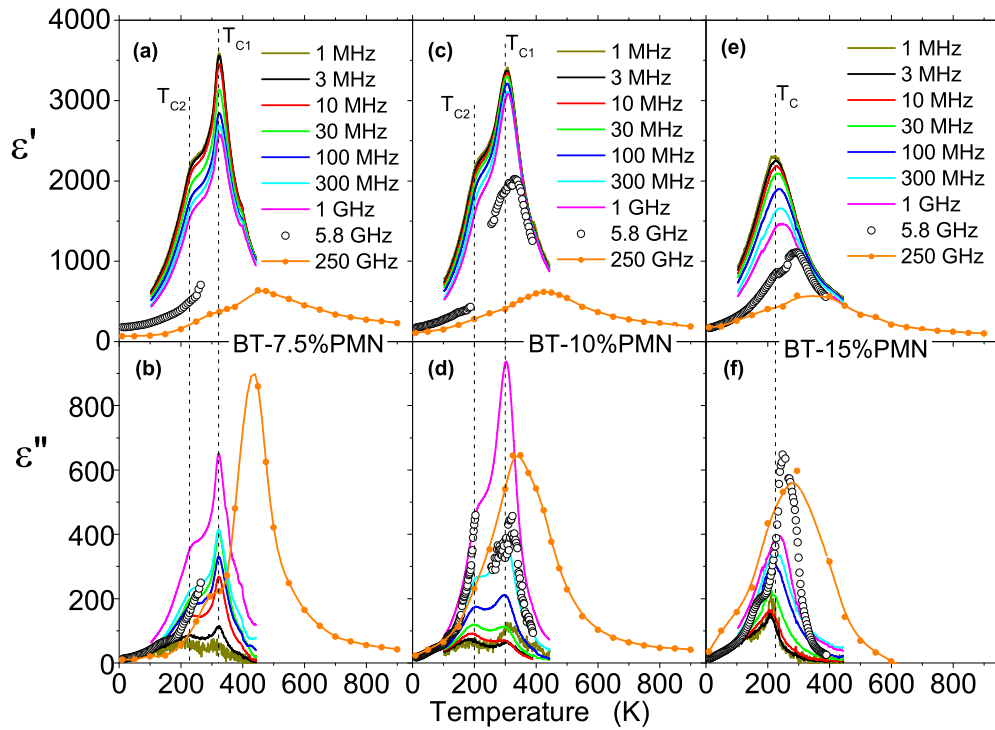


FIG. 2. Temperature dependences of the dielectric permittivity and loss of (a), (b) BT-7.5%PMN, (c), (d) BT-10%PMN, and (e), (f) BT-15%PMN ceramics at selected frequencies. T_1 and T_2 denote the temperatures of the low-frequency permittivity maxima, corresponding to the cubic-tetragonal and tetragonal-rhombohedral phase transitions, respectively; T_C denotes the temperature of the permittivity maximum corresponding to the cubic-rhombohedral phase transition in BT-15%PMN [22].

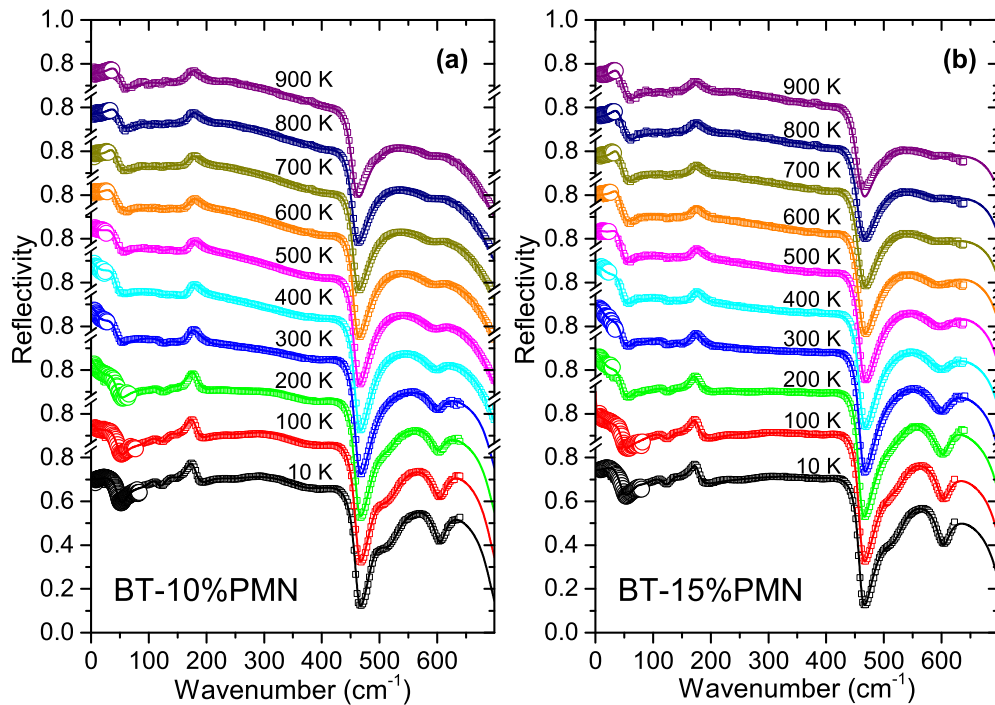


FIG. 3. IR (squares) and THz (circles) reflectivity spectra of (a) BT-10%PMN and (b) BT-15%PMN, and their fits (lines) using Eqs. (1) and (2) at selected temperatures.

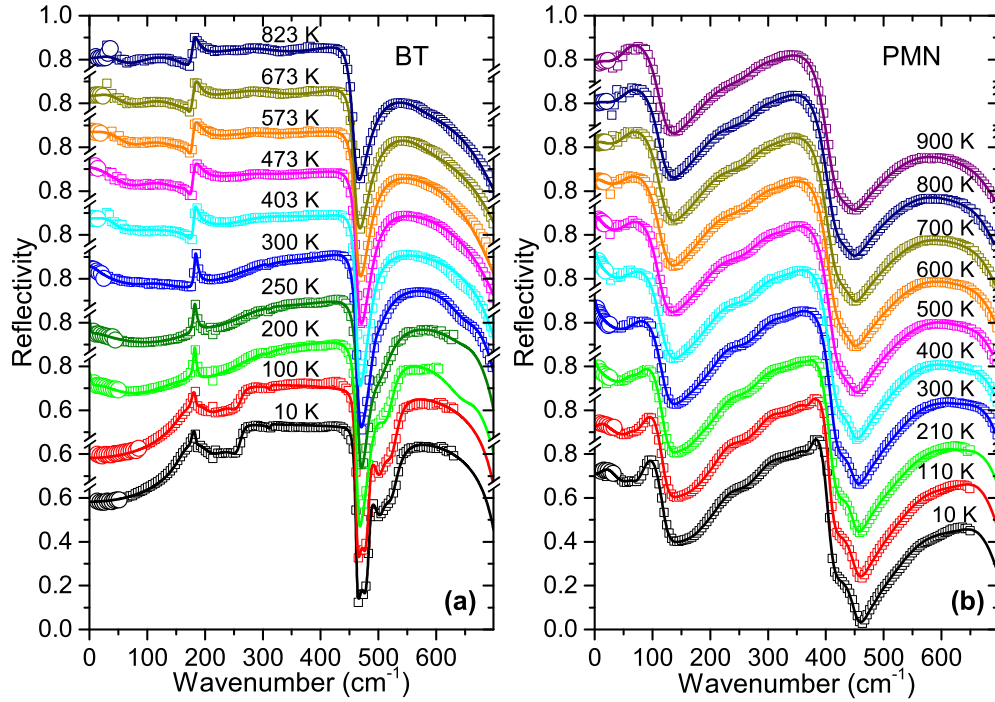


FIG. 4. IR (squares) and THz (circles) reflectivity spectra of (a) BT and (b) PMN, and their fits (lines) using Eqs. (1) and (2) at selected temperatures. Based on our data in Refs. [14,24–27].

For the discussion of IR-THz data, it is useful to present also the IR conductivity spectra $\sigma'(\omega) = 2\pi\epsilon_0\omega\epsilon''(\omega)$, which have the advantage that the area under each conductivity vs frequency peak is proportional to the corresponding mode

strength (f_j) [34]:

$$f_j = \Delta\epsilon_j\omega_{TOj}^2 = \epsilon_\infty \frac{\prod_k (\omega_{LOk}^2 - \omega_{TOj}^2)}{\prod_{k \neq j} (\omega_{TOk}^2 - \omega_{TOj}^2)}. \quad (3)$$

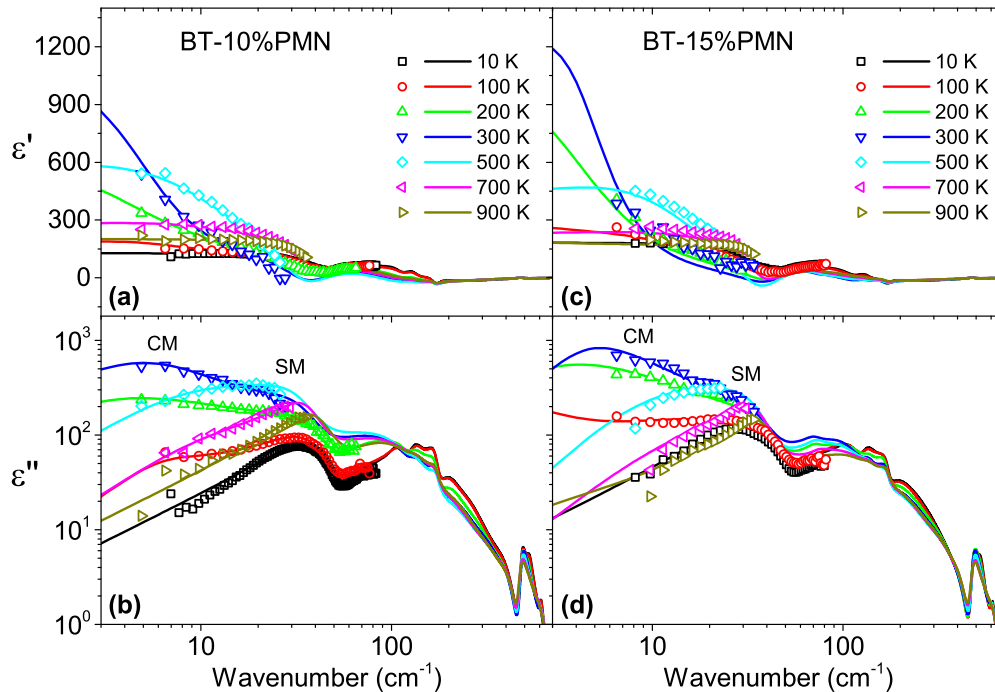


FIG. 5. Complex dielectric response (lines) evaluated from the IR-THz fit to reflectivity in Fig. 3 using Eqs. (1) and (2) for (a), (b) BT-10%PMN and of (c), (d) BT-15%PMN along with THz data (symbols).

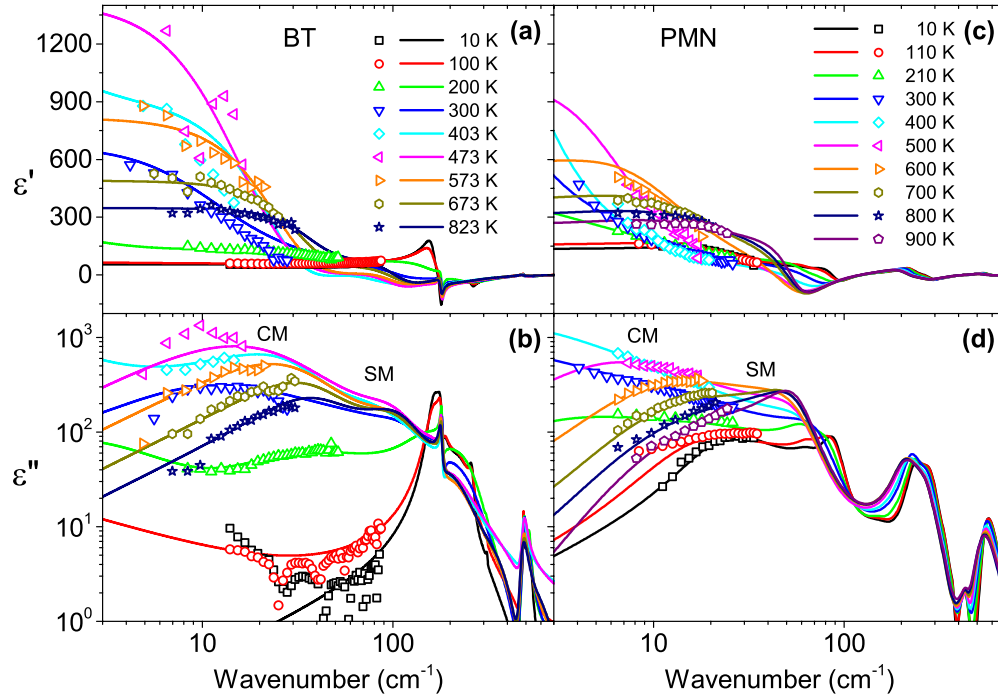


FIG. 6. Complex dielectric response (lines) obtained from the IR-THz fit to reflectivity for (a), (b) BT [24] and (c), (d) PMN [14] along with THz data (symbols).

The finite integral over the whole conductivity spectrum is proportional to the total electric charge taking part in all absorption processes [35]:

$$\int_0^{\infty} \sigma'(\omega) d\omega = \frac{\pi N e^2}{2 m}, \quad (4)$$

valid for one type of charges e of concentration N and effective mass m .

The conductivity spectra of BT-10%PMN and BT-15%PMN evaluated from their IR-THz dielectric response in Fig. 5 are shown in Fig. 7. Similarly, the conductivity spectra of BT and PMN evaluated from their IR-THz dielectric response in Fig. 6 are shown in Fig. 8.

V. ANALYSIS OF MW DIELECTRIC RESPONSE

For analysis of the dielectric response of the BT and BT-PMN ceramics at frequencies from 1 MHz to ~ 0.3 THz we used the sum of the IR response $\varepsilon_{IR}^*(\omega)$ described by Eq. (1) and the sum of phenomenological Cole-Cole relaxation terms [26]:

$$\begin{aligned} \varepsilon^*(\omega) &= \varepsilon'(\omega) - i\varepsilon''(\omega) \\ &= \varepsilon_{IR}^*(\omega) + \sum_j \frac{\Delta\varepsilon_j}{1 + (i\omega/\omega_{Rj})^{1-\alpha_j}}, \end{aligned} \quad (5)$$

where $\Delta\varepsilon_j$, ω_{Rj} , and $0 \leq \alpha_j \leq 1$ are the dielectric strength, mean relaxation frequency [at the maximum of dielectric loss function $\varepsilon''(\omega)$], and degree of broadening of the j th Cole-Cole relaxation, respectively. $\alpha_j = 0$ corresponds to the Debye relaxation; $\alpha_j \rightarrow 1$ describes the infinitely broad uni-

form distribution of Debye relaxations corresponding to the frequency-independent loss spectra.

Equation (5) formally expands the IR fit [Eq. (1)] to our whole frequency range 1 MHz–20 THz. However, it is not possible to fit the whole dielectric spectra together with a model formula of Eq. (5), because the relaxations yield unphysically high losses at high frequencies far above the loss peaks and do not fulfill the charge-sum rule [36], which requires the finite conductivity integral [Eq. (4)]. Therefore, in practice, we have used the MW fits [Eq. (5)] up to ~ 0.3 THz, while the IR fits [Eq. (1)] are used above ~ 0.3 THz. The experimental THz data are used in both IR and MW fits and provide smooth joining of both fitting models [Eqs. (1) and (5)].

Parameters of the lowest-frequency oscillator (corresponding to the CM) in the IR fit are not unambiguously defined by the THz data, especially at low temperatures (see Fig. 9). Accounting for the MW and THz experimental data, the MW fit could provide better estimate of the CM parameters. The resulting overall fitted spectra of BT-10%PMN and BT-15%PMN are shown in Figs. 9 and 10.

In a similar way, the broadband dielectric spectra of BT ceramics were also fitted by Eq. (5). The fits are shown in Figs. 11(a) and 11(b) together with the experimental data. For better comparison, dielectric spectra of all BT-PMN ceramics at the temperature of their permittivity maxima $\varepsilon'(T)$ are plotted in Figs. 11(c) and 11(d) together with the spectrum of PMN at 290 K from Ref. [14]. Dielectric spectra of BT-7.5%PMN are similar to that of BT-10%PMN except for the presence of the R2 relaxation which is observed in BT and PMN, but is absent in BT-10%PMN and BT-15%PMN.

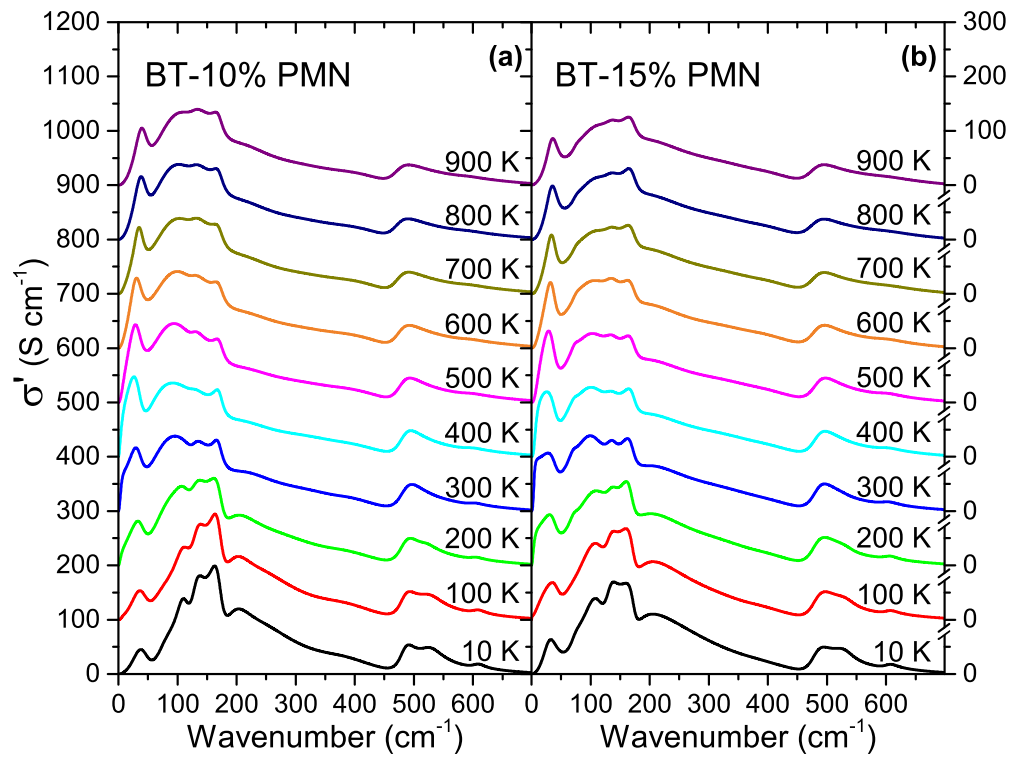


FIG. 7. Conductivity spectra of (a) BT-10%PMN and (b) BT-15%PMN evaluated from their IR-THz dielectric response in Fig. 5. Each spectrum is shifted by 100 S cm^{-1} with respect to the previous one.

VI. DISCUSSION

Comparison of the THz-IR dielectric spectra of BT-10%PMN and BT-15%PMN (Fig. 5) with those of BT and

PMN (Fig. 6) show that the response in both BT-PMN samples is rather similar but differs appreciably from that of pure BT and PMN, which also differ strongly from each other. The loss

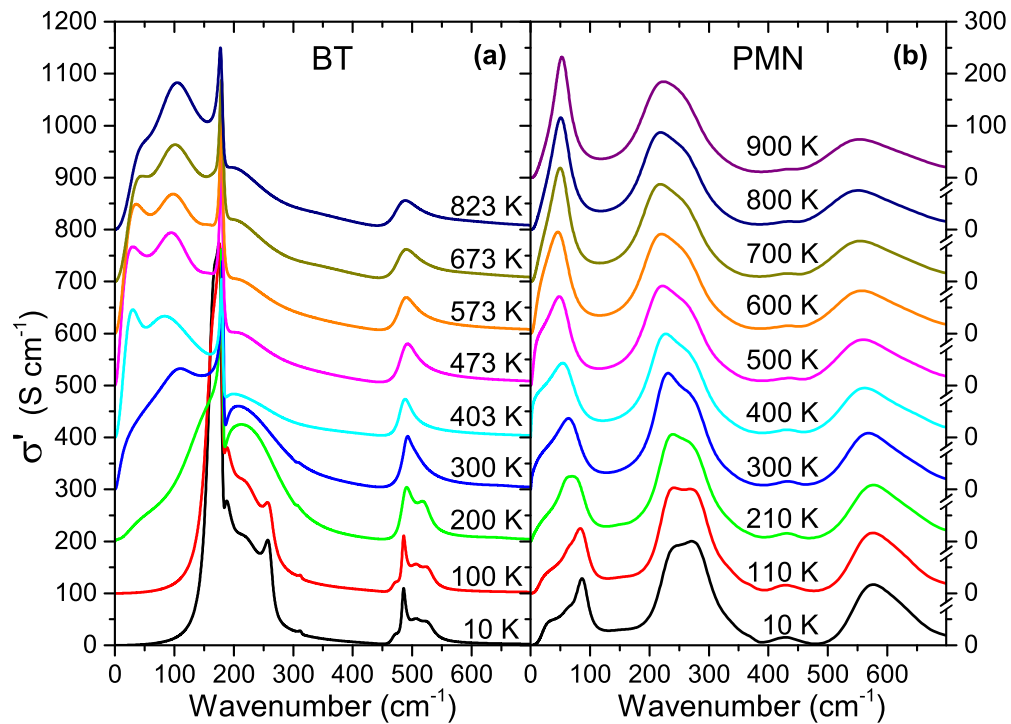


FIG. 8. Conductivity spectra of (a) BT and (b) PMN evaluated from their IR-THz dielectric response in Fig. 6. Each spectrum is shifted by 100 S cm^{-1} with respect to the previous one.

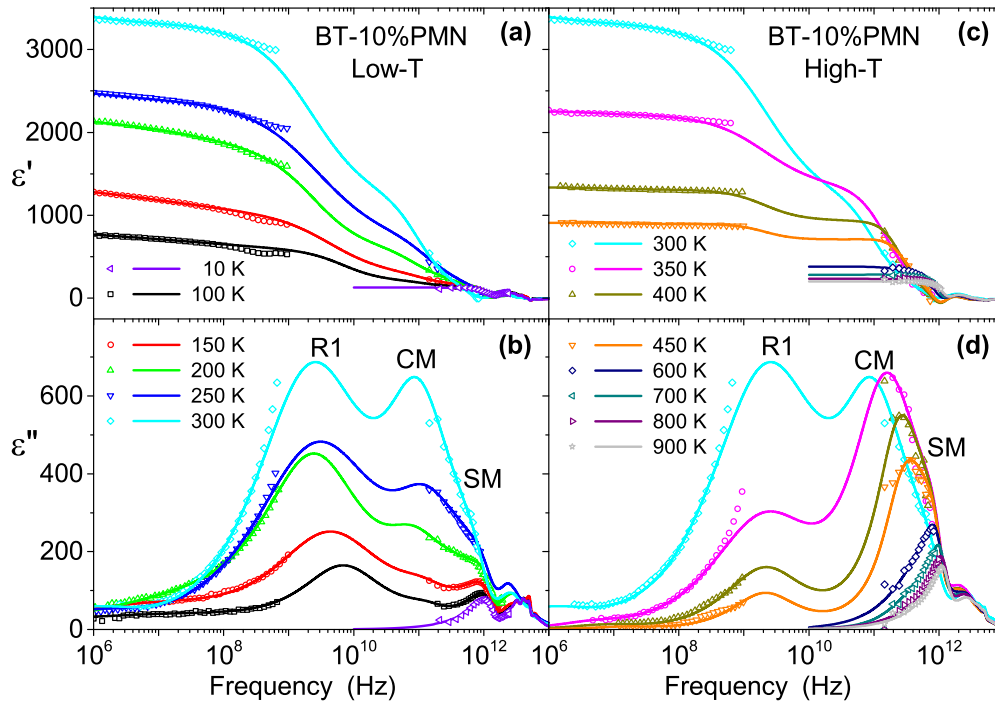


FIG. 9. Broadband spectra of (a), (c) dielectric permittivity and (b), (d) loss of the BT-10%PMN at (a), (b) low and (c), (d) high temperatures. Symbols denote experimental MW and THz points; lines correspond to the IR [Eq. (1)] and MW [Eq. (5)] fits. SM, CM, and R1 indicate the loss maxima of the corresponding modes. The CM and SM loss maxima are overlapped and, therefore, the mean SM frequency lies on the high-frequency wing of the CM maximum.

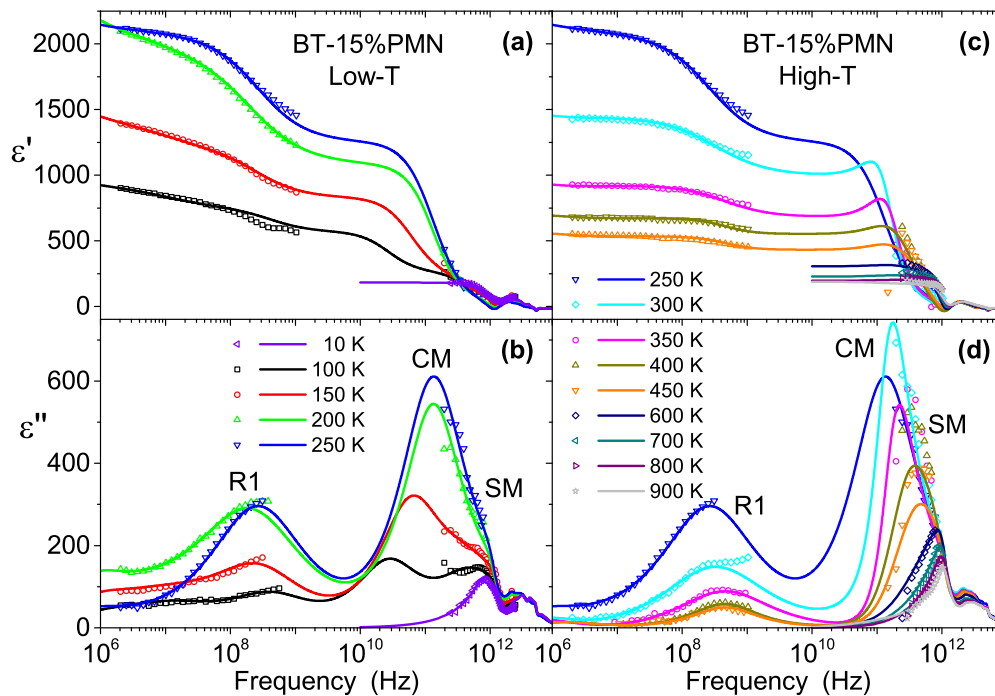


FIG. 10. Broadband spectra of (a), (c) dielectric permittivity and (b), (d) high temperatures. Symbols denote the experimental MW and THz points; lines correspond to the IR [Eq. (1)] and MW [Eq. (5)] fits. SM, CM, and R1 indicate the loss maxima of the corresponding modes. The CM and SM loss maxima are overlapped and, therefore, the mean SM frequency lies on the high-frequency wing of the CM maximum.

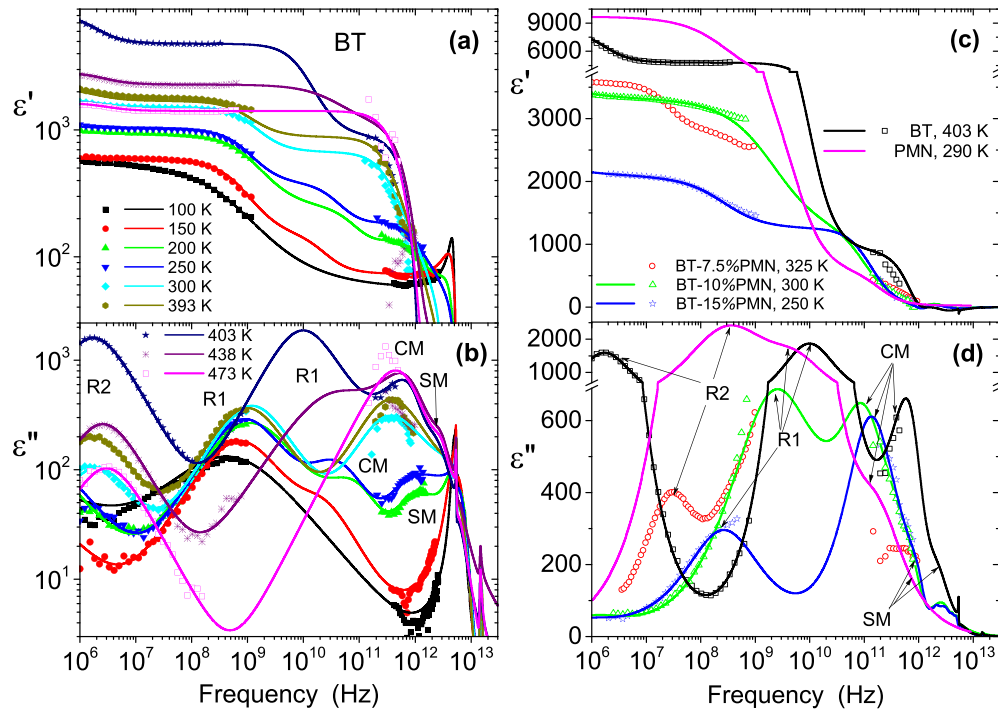


FIG. 11. Broadband spectra of (a) dielectric permittivity and (b) loss of the BT ceramics at selected temperatures. (c), (d) The permittivity and loss, respectively, of BT, BT-PMN ceramics, and PMN [14] at temperatures near their low-frequency permittivity maxima. Symbols denote the experimental MW and THz data; lines correspond to the MW [Eq. (5)] and IR [Eq. (1)] fits. SM, CM, R1, and R2 indicate the loss maxima of the corresponding modes.

response in BT-PMN is dominated by the split overdamped SM below $\sim 50 \text{ cm}^{-1}$ and another complex loss peak in the $100\text{--}300 \text{ cm}^{-1}$ range. The spectra are broader than those of BT and PMN, which is better seen from the linear conductivity spectra in Figs. 7 and 8. Whereas in BT the spectra become much sharper below the ferroelectric transition of $\sim 400 \text{ K}$, in BT-PMN the changes below the ferroelectric transitions are much weaker. This indicates a strong disorder down to low temperatures, caused by the PMN clusters which naturally remain frozen from rather high temperatures. Moreover, from structural data [22] it appears that the ferroelectric phases in our BT-PMN samples are coexisting with each other and with the cubic paraelectric phase, which also contributes to the spectra smearing. The spectra below $\sim 300 \text{ cm}^{-1}$ correspond to the two lower-frequency transverse optic phonon modes of the perovskite structure ABO_3 , so-called Slater and Last mode, whose eigenvectors consist of displacements of the B ions against the O_6 octahedra and A ions against the BO_6 octahedra, respectively [37]. The Slater mode is known to have much higher oscillator strength than the Last mode and its eigenvector dominates in the SM of BT [37], whereas in PMN, in analogy to PbTiO_3 [37], the Last eigenvector should dominate in the SM response. However, comparing the strengths of both PMN modes in the conductivity spectra in Fig. 8(b), it is seen that both eigenvectors are partly mixed together. In our BT-PMN samples, the modes below $\sim 300 \text{ cm}^{-1}$ are highly damped and split into several components, but do not show any pronounced temperature dependence, which makes their more detailed discussion difficult. We can assume that the conductivity peak separated below 50 cm^{-1} corresponds to

the SM of mixed Slater and Last eigenvector, but its softening is almost suppressed and its strength as well as softening is largely transferred to the CM component. This indicates a strong coupling between both the SM components. The remaining weaker conductivity response in the high-frequency $450\text{--}650 \text{ cm}^{-1}$ range can be attributed to so-called Axe mode in the ABO_3 perovskites, which corresponds to vibrations of the O ions only [37].

The dielectric response below $\sim 1 \text{ THz}$ of our BT-10%PMN and BT-15%PMN ceramics was well fitted by three excitations: SM, CM, and R1 relaxation. Dielectric spectra of the BT-7.5%PMN are similar to that of BT-10%PMN except for the second relaxation R2, present also in BT (Fig. 11), but absent in BT-10%PMN and BT-15%PMN. Temperature dependences of the THz and MW fit parameters of BT-10%PMN and BT-15%PMN at selected temperatures are shown in Fig. 12. For better comparison, in Fig. 13 we present similar parameters of the main high-frequency excitations of BT and PMN based on our results in Refs. [24,26,27] and [14], respectively. One can see that similar set of the high-frequency excitation (SM, CM, R1, R2) can fit the response of the ferroelectric and paraelectric BT, as well as the BT-PMN solid solutions and PMN. Let us compare the temperature dependences of the main parameters.

All the mode frequencies in Figs. 12 and 13 correspond to the loss maxima $\varepsilon''(\omega)$. In the case of overdamped CM, the $\omega_{\text{CM}}^2/\gamma_{\text{CM}}$ values are plotted, which are known to correspond well to the loss maxima, because they have better physical meaning and higher measured accuracy than the oscillator frequencies ω_{CM} [14]. The CM frequencies of BT, BT-10%PMN,

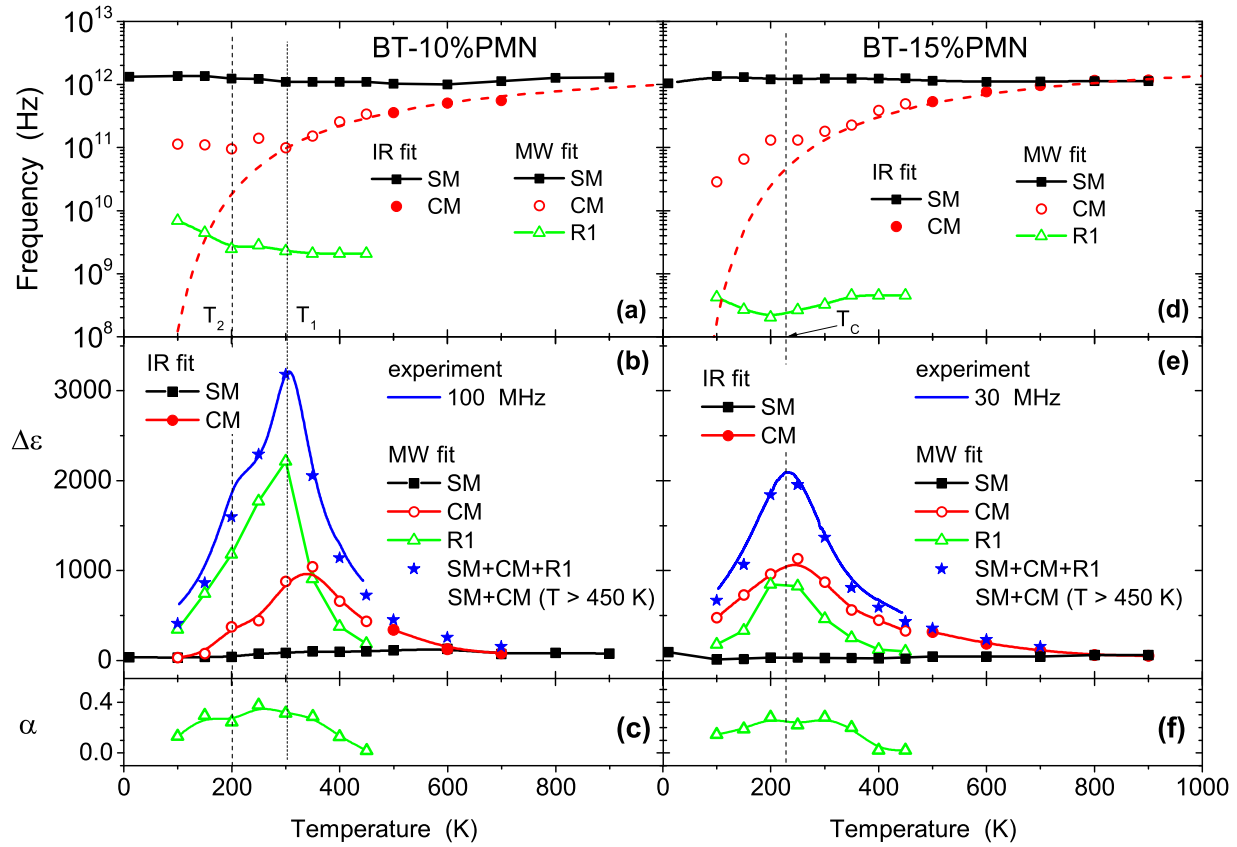


FIG. 12. Temperature dependences of the IR and MW fit parameters of (a)–(c) BT-10%PMN and (d)–(f) BT-15%PMN at selected temperatures. Dashed lines show the Arrhenius fits of the CM frequencies in the paraelectric phase. The SM parameters, obtained from the IR fit, were also used in the MW fit.

and BT-15%PMN in the paraelectric phase soften and follow the Arrhenius law (Figs. 12 and 13):

$$\omega_{\text{CM}} = \omega_0 \exp\left(-\frac{E}{T}\right), \quad (6)$$

with the same activation energy ($E = 1000$ K) and pre-exponential frequency $\omega_0 = 3\text{--}4$ THz. However, since the temperature region of validity is limited and rather high, the distinction from Vogel-Fulcher or other softening law is rather limited.

In the case of PMN, the lower-temperature Arrhenius fit of the R1 frequency ($E = 2350$ K and $\omega_0 = 15$ THz) fits surprisingly well also the CM frequency at high temperatures [Fig. 13(d)]. The R2 frequency of PMN follows the Vogel-Fulcher law

$$\omega_{R2} = \omega_0 \exp\left(-\frac{U}{T - T_{\text{VF}}}\right) \quad (7)$$

with the activation energy $U = 800$ K, freezing temperature $T_{\text{VF}} = 200$ K, and preexponential frequency $\omega_0 = 1$ THz. It represents the classical relaxation well known from the low-frequency dielectric measurements [12].

Concerning the BT, temperature dependence of the permittivity at 3 MHz [Fig. 13(b)] in the paraelectric phase follows very well the Curie-Weiss law

$$\varepsilon'(T) = C/(T - T_\theta) + \varepsilon_L \quad (8)$$

with the Curie-Weiss constant $C = 1.25 \times 10^5$ K (typical for BT ceramics), temperature-independent contribution $\varepsilon_L \approx 100$, and Curie-Weiss temperature $T_\theta = 383$ K. The same Curie-Weiss fit describes well the temperature dependence above 500 K of the $\Delta\varepsilon_{\text{ph+CM}}$ contribution solely [Fig. 13(b)]. The R1 relaxation undergoes a critical slowing down to T_θ , which correlates with the increase in its dielectric contribution and is in fact mainly responsible for the Curie-Weiss law close to ferroelectric transition temperature T_C , since the SM and CM frequencies do not soften sufficiently to account for the whole permittivity maximum. The R1 frequency above T_C sharply increases on heating, merges into the CM branch and can be well fitted with a combination of the Arrhenius law and critical slowing down of the preexponential frequency, as previously used for the relaxation in PMN-35%PbTiO₃ ceramics [38]:

$$\omega_{R1} = \omega_0(T - T_\theta) \exp\left(-\frac{E}{T}\right), \quad (9)$$

with the activation energy $E = 1900$ K, $\omega_0 = 0.1$ THz, and the critical temperature $T_\theta = 383$ K, fixed from the Curie-Weiss law. Similar relaxation was observed also in the BT single crystals [39] and ceramics [40] above T_C and was assigned to dynamics of the critical polar clusters of the off-centered Ti ions due to the well-known mixed displacive and order-disorder nature of the ferroelectric transition in BT.

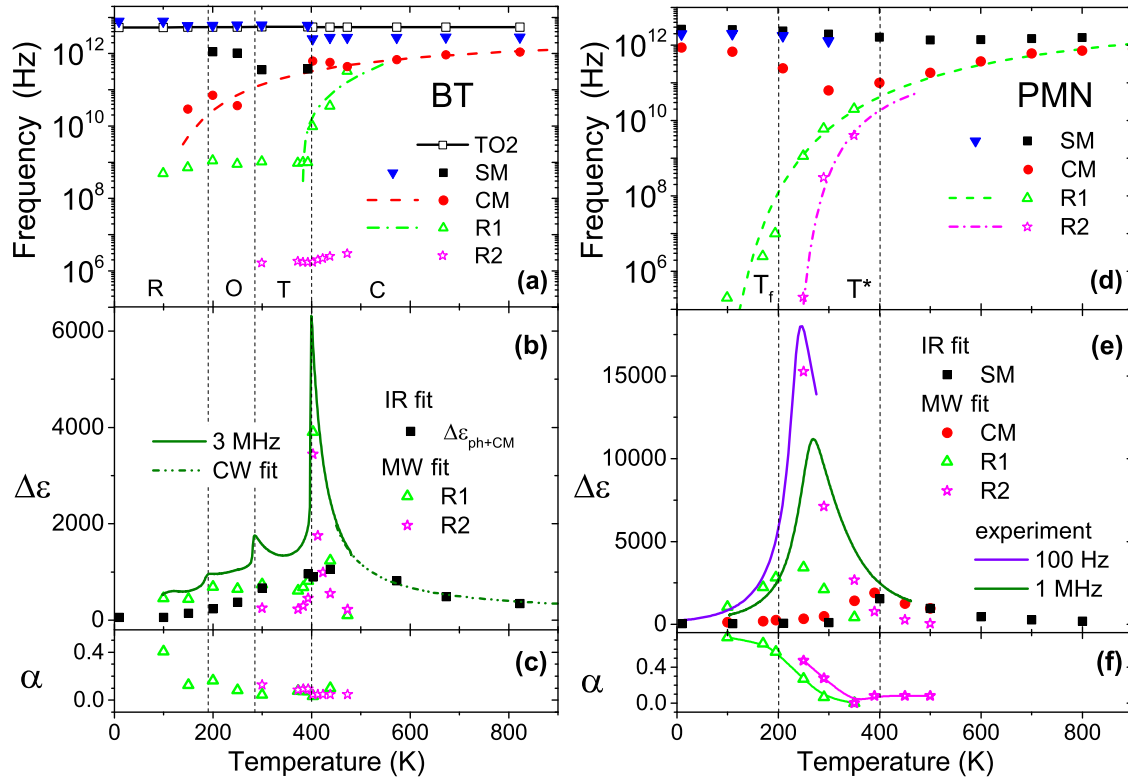


FIG. 13. Temperature dependences of the IR and MW fit parameters of (a)–(c) BT and (d)–(f) PMN. SM and CM parameters of PMN are taken from Ref. [14]. Dashed lines show (a) the Arrhenius fits of the CM in BT and (d) the R1 frequencies in PMN. Dashed-dotted lines show (d) the Vogel-Fulcher fit of the R2 frequency in PMN and (a) the mixed Arrhenius-critical slowing down fit [Eq. (6)] of the R1 frequency of BT in the paraelectric phase. Dielectric contribution $\Delta\epsilon_{\text{ph+CM}}$ in (b) includes contributions of CM, SM, and other IR phonons. Dashed-dotted-dotted lines in (b) show the Curie-Weiss fit of BT in the paraelectric phase at 3 MHz. In (a)–(c) we have marked the temperature regions of the rhombohedral (R), orthorhombic (O), tetragonal (T), and cubic (C) phases of BT; in (d)–(f) we have marked the freezing, $T_f \approx 200$ K, and characteristic $T^* \approx 400$ K temperatures of PMN.

Below T_C , the relaxations in BT and BT-PMN are not thermally activated (show no Arrhenius nor Vogel-Fulcher freezing) and their frequencies are only weakly temperature dependent. Without going into quantitative details, this is compatible with their assignment to smeared piezoelectric resonances or emission of acoustic waves at grain boundaries and/or ferroelastic domain walls [41]. Above T_C , the R1 frequencies of BT-PMN as well as R2 in BT remain also only weakly temperature dependent. However, their increase in the dielectric strengths $\Delta\epsilon$ towards T_C clearly shows their coupling to the strongly softening R1 in the case of BT and to the CM in the case of BT-PMN. Dielectric strengths $\Delta\epsilon$ of the CM, R1, and R2 are responsible for the permittivity vs temperature maxima in PMN and BT-PMN, while the SM contribution to permittivity becomes significant only at high temperatures, far above the permittivity maximum. In the case of BT ceramics, the SM and CM fully account for the permittivity above ~ 500 K as in the BT single crystals [42].

Since in BT and BT-PMN the SM, CM, R1, and R2 excitations completely describe the high-frequency response, the main dielectric dispersion at $T > 100$ K takes place above 1 MHz. In PMN, however, the dynamics expands to quite low frequencies on cooling below 200 K [13], and the R1, R2 contributions dominate in the low-temperature low-frequency response, not studied here. Parameter α characterizing the broadening of the R1 and R2 spectra increases on cooling

from almost zero at ~ 500 K to $\alpha \sim 0.4$ (in the case of BT and BT-PMN) or to quite high $\alpha \sim 0.8$ in the case of PMN, so that R1 and R2 broaden on cooling, but only in PMN they broaden and shift to the low-frequency range below 1 MHz. In BT-PMN the relaxations show no PMN-like slowing down [Figs. 13(d)–13(f)], but remind more the MW dielectric dispersion observed in the ferroelectric phases of the BT ceramics [Figs. 13(a)–13(c)]. Moreover, it is influenced by the possible coexistence of ferroelectric and paraelectric phases [22]. Concluding all the discussed features, which are not compatible with the classical relaxor ferroelectric behavior, the BT-PMN ceramics can be considered as ferroelectrics with the diffuse phase transitions rather than relaxor ferroelectrics.

VII. CONCLUSION

The broadband high-frequency dielectric measurements (1 MHz–20 THz) of three BT-100x%PMN ceramic solid solutions ($x = 0.075, 0.1, \text{ and } 0.15$) in a broad temperature range (10–900 K) were performed, fitted, and compared with the corresponding spectra of the undoped BT and PMN ceramics, based on our previously published data and new fits of the BT ceramics spectra. No phonon mode softening and no sharp temperature changes were observed in the IR spectra on passing through the ferroelectric phase transitions, but a

softening overdamped central mode was revealed in the paraelectric phase below the THz range, partly responsible for the dielectric maximum near T_C . Another comparable contribution to the permittivity vs temperature maximum was due to a microwave relaxation, which, however, did not freeze in, was not thermally activated, and remained above ~ 100 MHz in the ferroelectric phases down to 100 K. In analogy to BT ceramics [42] it was assigned to piezoresonances and/or acoustic wave emission on grain boundaries, frozen clusters, and nanodomains. Since this is not compatible with the relaxor ferroelectric behavior, the BT-PMN ceramics should be considered as ferroelectrics with diffuse phase transitions. On the other hand, in the paraelectric phase of BT, the soft and

central modes soften only partially towards T_C and two additional dielectric relaxations below 500 K, are substantially responsible for dielectric anomaly at T_C .

ACKNOWLEDGMENTS

This work is supported by the Czech Science Foundation (Project No. LA 20–20326L), by the Czech Academy of Sciences (Project No. PAN-17-14), and by Operational Programme Research, Development and Education financed by European Structural and Investment Funds and the Czech Ministry of Education, Youth and Sports (Project No. SOLID 21- CZ.02.1.01/0.0/0.0/16_019/0000760).

-
- [1] M. Acosta, N. Novak, V. Rojas, S. Patel, R. Vaish, J. Koruza, G. A. Rossetti, and J. Rödel, BaTiO₃-based piezoelectrics: Fundamentals, current status, and perspectives, *Appl. Phys. Rev.* **4**, 041305 (2017).
- [2] J. Wu, Perovskite lead-free piezoelectric ceramics, *J. Appl. Phys.* **127**, 190901 (2020).
- [3] D. H. Kang and K. H. Yoon, Stabilization of the perovskite phase and dielectric-properties in the Pb(Mg_{1/3}Nb_{2/3})O₃-BaTiO₃ system, *J. Mater. Sci.* **26**, 56 (1991).
- [4] Z. R. Li, Q. Li, L. Y. Zhang, and X. Yao, Dielectric properties and transition temperature of ceramics in the Pb(Mg_{1/3}Nb_{2/3})O₃-BaTiO₃ system, *Ferroelectrics* **262**, 47 (2001).
- [5] P. D. Spagnol, M. A. Zaghete, C. O. Paiva-Santos, A. V. C. Andrade, A. A. Cavalheiro, S. M. Tebcherani, and J. A. Varela, Effect of barium titanate seed particles on the sintering and lattice parameters in PbMg_{1/3}Nb_{2/3}O₃ ceramics, *J. Mater. Res.* **17**, 620 (2002).
- [6] M. E. Lines and A. M. Glass, *Principles and Applications of Ferroelectrics and Related Materials* (Oxford University Press, Oxford, 2001).
- [7] R. Comes, M. Lambert, and A. Guinier, Chain structure of BaTiO₃ and KNbO₃, *Solid State Commun.* **6**, 715 (1968).
- [8] A. Ziębińska, D. Rytz, K. Szot, M. Gorny, and K. Roleder: Birefringence above T_c in single crystals of barium titanate, *J. Phys.: Condens. Matter* **20**, 142202 (2008).
- [9] J. Hlinka, T. Ostapchuk, D. Nuzhnyy, J. Petzelt, P. Kuzel, C. Kadlec, P. Vanek, I. Ponomareva, and L. Bellaiche, Coexistence of the Phonon and Relaxation Soft Modes in the Terahertz Dielectric Response of Tetragonal BaTiO₃, *Phys. Rev. Lett.* **101**, 167402 (2008).
- [10] F. Jona and G. Shirane, *Ferroelectric Crystals* (Pergamon Press, Oxford, 1962).
- [11] P. Bonneau, P. Garnier, G. Calvarin, E. Husson, J. R. Gavarri, A. W. Hewat, and A. Morell, X-ray and neutron-diffraction studies of the diffuse phase-transition in PbMg_{1/3}Nb_{2/3}O₃ ceramics, *J. Solid State Chem.* **91**, 350 (1991).
- [12] A. A. Bokov and Z. G. Ye, Recent progress in relaxor ferroelectrics with perovskite structure, *J. Mater. Sci.* **41**, 31 (2006).
- [13] V. Bovtun, S. Veljko, S. Kamba, J. Petzelt, S. Vakhrushev, Y. Yakymenko, K. Brinkman, and N. Setter, Broad-band dielectric response of PbMg_{1/3}Nb_{2/3}O₃ relaxor ferroelectrics: Single crystals, ceramics and thin films, *J. Eur. Ceram. Soc.* **26**, 2867 (2006).
- [14] D. Nuzhnyy, J. Petzelt, V. Bovtun, M. Kempa, S. Kamba, J. Hlinka, and B. Hehlen, Infrared, terahertz, and microwave spectroscopy of the soft and central modes in Pb(Mg_{1/3}Nb_{2/3})O₃, *Phys. Rev. B* **96**, 174113 (2017).
- [15] Z.-G. Ye and H. Schmid, Optical, dielectric and polarization studies of the electric field-induced phase transition in Pb(Mg_{1/3}Nb_{2/3})O₃ [PMN], *Ferroelectrics* **145**, 83 (1993).
- [16] K. Hirota, Z. G. Ye, S. Wakimoto, P. M. Gehring, and G. Shirane, Neutron diffuse scattering from polar nanoregions in the relaxor Pb(Mg_{1/3}Nb_{2/3})O₃, *Phys. Rev. B* **65**, 104105 (2002).
- [17] S. Wakimoto, C. Stock, Z. G. Ye, W. Chen, P. M. Gehring, and G. Shirane, Mode coupling and polar nanoregions in the relaxor ferroelectric Pb(Mg_{1/3}Nb_{2/3})O₃, *Phys. Rev. B* **66**, 224102 (2002).
- [18] B. Dkhil, J. M. Kiat, G. Calvarin, G. Baldinozzi, S. B. Vakhrushev, and E. Suard, Local and long range polar order in the relaxor-ferroelectric compounds PbMg_{1/3}Nb_{2/3}O₃ and PbMg_{0.3}Nb_{0.6}Ti_{0.1}O₃, *Phys. Rev. B* **65**, 024104 (2002).
- [19] S. Vakhrushev, S. Zhukov, G. Fetisov, and V. Chernyshov, The high-temperature structure of lead magnoniobate, *J. Phys.: Condens. Matter* **6**, 4021 (1994).
- [20] N. de Mathan, E. Husson, G. Calvarin, J. R. Gavarri, A. W. Hewat, and A. Morell, A structural model for the relaxor PbMg_{1/3}Nb_{2/3}O₃ at 5 K, *J. Phys.: Condens. Matter* **3**, 8159 (1991).
- [21] M. Eremenko, V. Krayzman, A. Bosak, H. Y. Playford, K. W. Chapman, J. C. Woicik, B. Ravel, and I. Levin, Local atomic order and hierarchical polar nanoregions in a classical relaxor ferroelectric, *Nat. Commun.* **10**, 2728 (2019).
- [22] J. Suchanicz, K. Świerczek, E. Nogas-Ćwikiel, K. Konieczny, and D. Sitko, PbMg_{1/3}Nb_{2/3}O₃-doping effects on structural, thermal, Raman, dielectric and ferroelectric properties of BaTiO₃ ceramics, *J. Eur. Ceram. Soc.* **35**, 1777 (2015).
- [23] J. Suchanicz, M. Karpierz, K. Konieczny, and K. Kluczewska, Effect of PMN addition on the structural, dielectric and ferroelectric properties of BT ceramics, *Ferroelectrics* **497**, 100 (2016).
- [24] T. Ostapchuk, J. Petzelt, M. Savinov, V. Buscaglia, and L. Mitoseriu, Grain-size effect in BaTiO₃ ceramics: Study by far infrared spectroscopy, *Phase Trans.* **79**, 361 (2006).
- [25] J. Petzelt, D. Nuzhnyy, M. Savinov, V. Bovtun, M. Kempa, T. Ostapchuk, J. Hlinka, G. Canu, and V. Buscaglia, Broad-band dielectric spectroscopy of Ba(Zr, Ti)O₃: Dynamics of

- relaxors and diffuse ferroelectrics, *Ferroelectrics* **469**, 14 (2014).
- [26] D. Nuzhnyy, J. Petzelt, M. Savinov, T. Ostapchuk, V. Bovtun, M. Kempa, J. Hlinka, V. Buscaglia, M. T. Buscaglia, and P. Nanni, Broadband dielectric response of Ba(Zr, Ti)O₃ ceramics: From incipient via relaxor and diffuse up to classical ferroelectric behavior, *Phys. Rev. B* **86**, 014106 (2012).
- [27] D. Nuzhnyy, J. Petzelt, V. Bovtun, T. Ostapchuk, M. Savinov, M. Kempa, P. Bednyakov, L. Fernández-García, T. Rodríguez-Suarez, and J. L. Menéndez, Broadband dielectric spectroscopy of standard and core-shell BaTiO₃-NiO ceramic composites compared to the BaTiO₃ ceramics, *Ferroelectrics* **500**, 1 (2016).
- [28] V. Bovtun, S. Kamba, A. Pashkin, M. Savinov, P. Samoukhina, J. Petzelt, I. P. Bykov, and M. D. Glinchuk, Central-Peak Components and Polar Soft Mode in Relaxor PbMg_{1/3}Nb_{2/3}O₃ Crystals, *Ferroelectrics* **298**, 23 (2004).
- [29] S. Kamba, D. Nuzhnyy, S. Denisov, S. Veljko, V. Bovtun, M. Savinov, J. Petzelt, M. Kalnberga, and A. Sternberg, Quantum paraelectric behavior of pyrochlore Pb_{1.83}Mg_{0.29}Nb_{1.71}O_{6.39}, *Phys. Rev. B* **76**, 054125 (2007).
- [30] P. Kužel and J. Petzelt, Time-resolved terahertz transmission spectroscopy of dielectrics, *Ferroelectrics* **239**, 79 (2000).
- [31] V. Bovtun, V. Pashkov, M. Kempa, S. Kamba, A. Eremenko, V. Molchanov, Y. Poplavko, Y. Yakymenko, J. H. Lee, and D. G. Schlom, An electrode-free method of characterizing the microwave dielectric properties of high-permittivity thin films, *J. Appl. Phys.* **109**, 024106 (2011).
- [32] V. Bovtun, S. Veljko, A. Axelsson, S. Kamba, N. Alford, and J. Petzelt, Microwave characterization of thin ferroelectric films without electrodes by composite dielectric resonator, *Integrated Ferroelectrics* **98**, 53 (2008).
- [33] J. Krupka, Frequency domain complex permittivity measurements at microwave frequencies, *Meas. Sci. Technol.* **17**, R55 (2006).
- [34] F. Gervais, in *Infrared and Millimeter Waves*, edited by K. J. Button (Academic Press, New York, 1983), Vol. 8, pp. 279–339.
- [35] J. Petzelt and V. Dvořák, in *Vibrational Spectroscopy of Phase Transitions*, edited by Z. Iqbal and F. J. Owens (Academic Press, Orlando, 1984), pp. 55–151.
- [36] J. Petzelt, D. Nuzhnyy, V. Bovtun, M. Savinov, M. Kempa, and I. Rychetský, Broadband dielectric and conductivity spectroscopy of inhomogeneous and composite conductors, *Phys. Status Solidi A* **210**, 2259 (2013).
- [37] J. Hlinka, J. Petzelt, S. Kamba, D. Noujni, and T. Ostapchuk, Infrared dielectric response of relaxor ferroelectrics, *Phase Trans.* **79**, 41 (2006).
- [38] V. Bovtun, S. Kamba, S. Veljko, D. Nuzhnyy, J. Kroupa, M. Savinov, P. Vaněk, J. Petzelt, J. Holc, M. Kosec, H. Amorín, and M. Alguero, Broadband dielectric spectroscopy of phonons and polar nanoclusters in PbMg_{1/3}Nb_{2/3}O₃ 35%PbTiO₃ ceramics: Grain size effects, *Phys. Rev. B* **79**, 104111 (2009).
- [39] M. Maglione, R. Bohmer, A. Loidl, and U. T. Hochli, Polar relaxation mode in pure and iron-doped barium titanate, *Phys. Rev. B* **40**, 11441 (1989).
- [40] T. Teranishi, T. Hoshina, H. Takeda, and T. Tsurumi, Wide band dielectric spectroscopy at ferroelectric phase transition of BaTiO₃ ceramics, *Jpn. J. Appl. Phys.* **49**, 041506 (2010).
- [41] G. Arlt, U. Bottger, and S. Witte, Dielectric dispersion of ferroelectric ceramics and single crystals at microwave frequencies, *Ann. Phys.* **3**, 578 (1994).
- [42] I. Ponomareva, L. Bellaiche, T. Ostapchuk, J. Hlinka, and J. Petzelt, Terahertz dielectric response of cubic BaTiO₃, *Phys. Rev. B* **77**, 012102 (2008).